Characteristics of Gas Pockets in Fluidized Beds

GEORGE YASUI and L. N. JOHANSON

University of Washington, Seattle, Washington

Some characteristics of gas pockets rising through beds of fluidized solids have been measured directly with a light probe technique. The vertical thickness, numerical frequency, and rate of rise of the bubbles were obtained from oscillographs of dual probe signals. Room-temperature air at 1-atm. pressure was used in 4- and 6-in. columns. Glass beads, a crushed rock, commercial cracking catalysts, coal, and hollow resin spheres were studied in particle sizes from 12-μ fluid cracking catalyst to 450-μ coal.

Vertical bubble thickness was found to increase with particle size, distance above the bed support, and gas velocity. Size growth upon rising was mainly the result of coalescence of bubbles. The rise velocity ranged from 1 to 2 ft./sec., relatively unaffected by operating conditions. Bubble frequency decreased with height above the bed support owing to coalescence. Total bed-depth variation from 1.0 to 2.5 ft. did not significantly influence the results, which should be of interest in studying gas by-passing in fluidized beds and predicting the slugging behavior and fluidization uniformity.

Literature about fluidized-solids technology in the fields of heat transfer, mass transfer, and reaction kinetics is building up rapidly. As insight is gained of the mechanism of fluidization resulting from such studies, it becomes more appararent that the nature of the "pockets," or "bubbles," of gas passing upward through a fluidized bed must be more completely determined. A generalization of the heat and mass transfer results now available may well depend upon such increased knowledge of these gas pockets.

In this work the terms *bubble* and *pocket* are used with complete interchangeability, mainly because the term *bubble*, representing the dilute phase of gas-fluidized beds is fairly well entrenched in the literature. From a semantic viewpoint the term *pocket* may be preferable to some, since there is no real phase boundary separating this gas from other gas within the fluidized bed.

The consideration of the use of fluidized beds for nuclear reactors has demonstrated another need for such information (*1*). In calculations for the design of such a reactor for neutron balance, voids or variation of solids density within the bed would be of paramount importance.

The present work was undertaken as an initial study to determine directly the size and size distribution, the numerical frequency, the rate of rise of such bubbles, and the process variables influencing them. The method is based upon the transmission of light between small probes submerged within the fluidized bed and conversion of the light signal to electrical impulses which are amplified and recorded.

Other techniques have been used in attempts to record the nature of the dense and disperse phases in a gas-fluidized bed or the extent to which the system deviates from the *smooth* or *particulate* fluidization observed in solids fluidized by liquids. The degree to which a system approaches such an idealized, smooth fluidization model has been termed *uniformity of fluidization* (*2*). Electrical capacitance probes (*2*, *3*), pressure-sensitive strain gauges (*4*), X-rays (*5*, *6*), viscometers (*7*, *8*, *9*), and surface-tension measurements (*10*) have all been used to measure this quality of fluidization. The results obtained have been very helpful in making qualitative comparisons of fluidized beds. Because of the indirect nature of the observation, however, it has not been possible, with the exception of X-ray techniques (*5*), to utilize them to obtain properties of individual bubbles.

Photographs of these disperse regions in fluidized beds have been made by Mathis and Watson (*11*) and Ohmae and Furukawa (*12*). Mathis and Watson utilized their data by scanning still photographs to obtain integrated densitometer values as a measure of fluidization quality, analogous to the work previously noted.

Direct evidence of the quantitative relation between the amount of gas in the form of bubbles and the inlet gas velocity was reported by Ohmae and Furukawa (*12*). High-speed photographs of air bubbles in beds of fluidized polyvinyl-acetate resin and of air bubbles in a glycerin solution having the same viscosity as the fluid bed of solids were examined. The behavior of bubbles in fluidized solids was said to be analogous to that in the liquid glycerin system. Small bubbles were initially formed just above the screen support and then grew in size by coalescing during their ascent. The frequency of bubbles therefore decreased with height above the bed support. A plot of volumetric flow rate of air bubbles vs. superficial air velocity under nonslugging conditions shows a family of slightly curved, nearly parallel lines representing the data for various diameters of the resin particles. For slugging conditions nonparallel straight lines with much steeper slopes were obtained. The size of the rectangular glass column used by Ohmae and Furukawa was not specified. Air-bubble volumetric flow rate was found to increase with increase in the ratio of L/D.

The results of Ohmae and Furukawa and also of Mathis and Watson were obtained by using flat-plate-walled columns, with the gas pockets rising adjacent to the glass wall. It is doubtful whether such data could be safely assumed to represent conditions within a larger fluidized bed, in which the gas pocket is not contacting the wall.

The current work was undertaken to determine properties, particularly of the gas pockets, which are not in contact with the column wall and which would therefore ordinarily not be visible externally. Such pockets however should be more representative of conditions within a larger fluidized bed than those at the wall. It was recognized at the outset that gas bubbles or pockets would vary considerably in size, shape, frequency of occurrence, position, and rise speed. Results for a given set of operating conditions thus would have to be based upon sufficient measurements of individual bubbles to allow significant differences between operating conditions to be revealed. The variables which could be expected to have a possible influence on bubble characteristics were

George Yasui is with Lockheed Aircraft Company, Palo Alto, California.

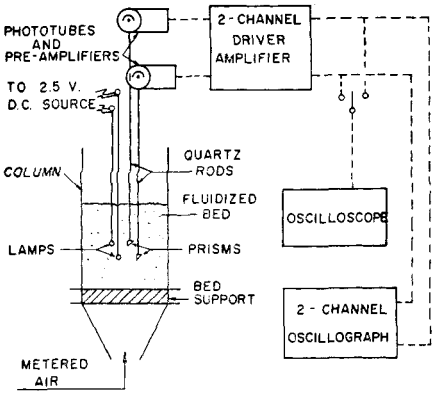

Fig. 1. Diagram of experimental apparatus.

many; it was not known initially which of these would be significant or whether they would act independently, that is, without interaction. This suggested a factorial design (*13*) for at least the early experiments, with randomized order of tests to minimize the influence of unknown variables. Complete details of the approach used are available elsewhere (*14*).

These considerations necessitated restricting the scope of the current investigation. In most of the work the vertical depth or thickness of a gas pocket, the speed of rise of the pocket, and the frequency with which the bubbles passed between the probes in a given position comprised the three items of data. Probe positions were restricted radially to the vertical column axis. Thorough investigation was made of three particle sizes of each of two materials. The effect of gas velocity, total (fixed) bed height, and the ratio of probe height above bed support to total height were investigated. The results of the last-named investigation were later converted to probe height above bed support when the height, rather than height ratio, proved to be the primary variable.

Additional tests supplemented studies of the major variables. The effect of column diameter; radial position of the probes; type of bed support; mixtures of sized particles; and solids of varying density, shape, and particle size were briefly investigated.

EXPERIMENTAL

Figure 1 is a schematic illustration of the apparatus. The sensing elements of a probe pair consisted of a light source and a light-reflecting prism. A $\frac{1}{8}$-in.-diameter Grain of Wheat tungsten-filament lamp, coupled to one end of a 3/32 in. O.D. metal tube through which ran an insulated wire lead, served as the light source. Facing the lamp was a small mirrored-glass prism cemented to one end of a 4-mm.-diameter clear-quartz rod which was wrapped with aluminum foil. With two pairs of probes, one above the other but offset in vertical planes approximately at right angles to each other, a rising gas bubble passing between the elements of the probes was detected by the lower and then the upper probe pair.

As the gas pocket occupied the space between the lamp and the prism, light was transmitted to the prism and reflected out through the quartz rod into a type-929 vacuum phototube; there it was converted into electrical signals, which subsequently were amplified through two stages of a D.C. balanced-bridge type of vacuum-tube circuit. A cathode follower circuit enabled the signals to operate the pen motor of a BL-202, Brush dual-channel oscillograph. An oscilloscope was used in the preliminary work.

The probe system was 40 in. long to allow placement at any level of a 3-ft.-deep fluidized bed. Distance between the lower and upper probe pairs, between light and prism of each probe, and radial position within the bed were all adjustable.

Four- and six-inch–inside-diameter Pyrex pipes were used as columns. In most of the experiments a $1\frac{1}{2}$-in.-thick porous ceramic disk supported the bed of solids. Separate experiments were conducted to test the effects of various porous plates and a 200-mesh screen. Laboratory air was filtered through cotton, and the air flow rate was controlled by a pair of pressure-reducing valves. Metering of the air flow rate was accomplished with rotameters or with orifice meters, depending on the range; these meters were calibrated by direct displacement of water at constant air-exhaust pressure. Air leaving the column was vented directly to the atmosphere.

Owing mainly to the inertia of the inking-pen system of the oscillograph, corrections were necessary for the measured oscillogram trace widths. About 1/100-sec. response time was noted for the pen to rise to or fall from the full amplitude upon the application or removal of an instantaneous input voltage to the oscillograph. In addition to the expected pen overshoot and undershoot the oscillograms showed that about 1/25 sec. elapsed while the pen oscillated back to the base line. On this basis the minimum interval between individual apparent bubble traces was chosen as 1/25 sec. Signal-trace amplitude was linear with input voltage except near the maximum height.

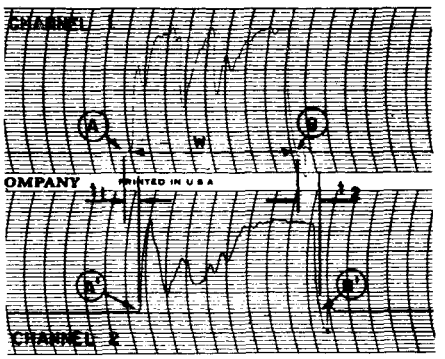

Fig. 2. Measurements obtained from signal traces with chart speed of 125 mm./sec.

By interposing the paper belt between the probes and recording the results in the same manner as was used for the fluidization work, one could calibrate the system for the corrected hole or bubble size and rise speed. Only the bubble-size correction, which was a function of both rise speed and hole size, was significant.

Materials

Most of the data were obtained on the glass-bead–air and the olivine-air systems, but other materials investigated were coal, hollow phenolic resin, magnetite catalyst, new UOP microspheroidal catalyst, and regenerated fluid-cracking (FCC) catalyst. The physical properties of the solids are given in Table 1. Unless otherwise specified, the surface-based diameter, obtained from experimental permeability data and use of Ergun's (*15*) equation, is used throughout this report. For purposes of comparison the 5 and 95% passing size and the mean surface diameters (*16*) based on the Tyler screen analysis of the various materials are also shown in Table 1.

Two mixtures of different-sized glass beads were also tested for their effects on bubble characteristics. Mix *C* was composed of an equal weight mixture of 75- and 175-μ glass beads; Mix *D* was an equal-weight mixture of 41-, 75-, and 175-μ beads.

A wide range in particle density was

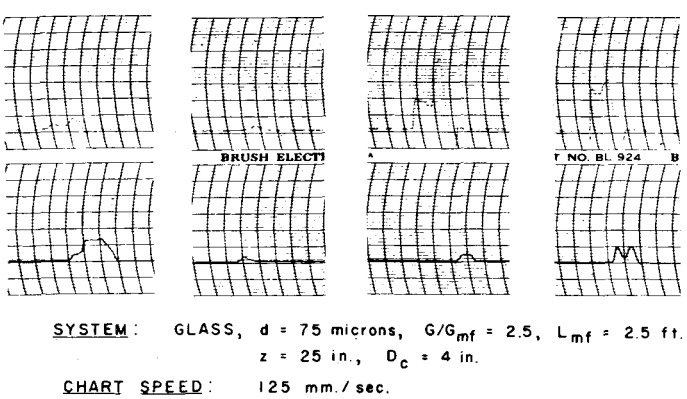

Fig. 3. Oscillogram traces for 75-μ glass beads at chart speed of 125 mm./sec.

The complete bubble-detecting and -recording system was calibrated under simulated conditions, wherein holes on an endless moving belt were measured. This moving belt consisted of a strip of paper in which were cut rectangular holes 0.25, 0.75, and 1.5 in. wide, spaced at known distances apart. The belt was driven by pulleys and a variable-speed motor.

afforded by the choice of solids used. The lightest material was the hollow phenolic resin with a particle density of 21 lb./cu. ft. and the heaviest was magnetite with a particle density of 304 lb./cu. ft. An attempt was made to remove the extreme fines by elutriation with air or water; however only partial success was obtained in the case of materials of wide size range.

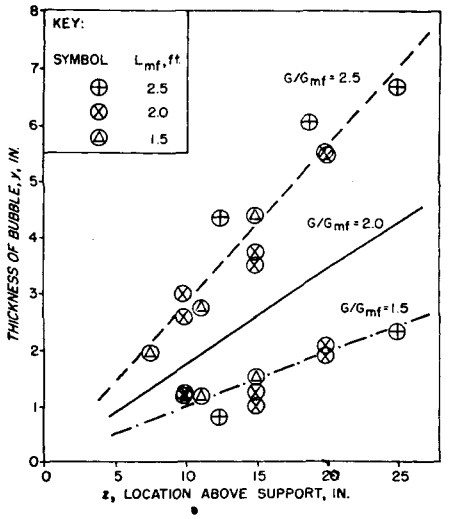

Fig. 4. Average vertical thickness of bubbles in 4 in. column, 242-μ glass beads.

TABLE 1. PHYSICAL PROPERTIES OF SOLID MATERIALS

Property	Material											
	Glass beads				Olivine rock			Hollow resin	UOP cat.	Coal	Fe_3O_4 cat.	Fluid cat.
Shape	Sphere				Irreg.			Sphere	Gran.	Gran.	Irreg.	Irreg.
Particle density, lb./cu. ft.	154	154	154	176	208	208	208	21	61	86	304	155
Avg. diam., μ (Permeability)*	41	75	175	242	42	100	150	81	60	450	70	12
(Mean surface)†	(57)	92	208	267	84	161	233	111	78	692	—	—
5% Retained size, μ		105	240	320	110	210	270	240	160	920	300	105
95% Retained size, μ		70	165	220	66	140	190	54	35	580	20	<30

*Calculated from permeability measurements, by Ergun's equation (*15*).
†Mean surface diameter (*16*) from Tyler screen analysis.

TABLE 2. COMPOSITE DATA: REPRESENTATIVE RESULTS

System code	Operating conditions					Average bubble data					
	Particle diameter, μ	Air flow G/G_{mf}	Air flow G, lb./(hr.)(sq. ft.)	Bed Ht. L, in.	Probe ht. Z, in.	Rise speed v, ft./sec.	Frequency n, 1/sec.	Thickness y, in.	Vol. Q_b, cu. ft./min.	G_b/G	y/z
G-11	41	2.0	8.8	30.8	12.5	1.10	0.38	0.33	0.05	0.28	0.026
G-11	41	2.5	11.0	18.5	7.5	1.41	0.42	0.41	0.08	0.36	0.055
G-13	75	2.5	25	24.0	10	1.37	2.54	0.83	0.92	1.96	0.083
GS-1	175	1.5	68	25	10	1.28	2.06	1.12	1.00	0.79	0.11
G-9	175	2.0	90	26	10	1.23	2.14	1.47	1.38	0.82	0.15
G-13	175	2.5	113	27.3	10	1.16	1.86	2.31	1.88	0.90	0.23
G-7	242	2.0	145	28	10	1.15	2.39	1.61	1.68	0.63	0.16
G-12	242	2.0	145	28	10	1.14	1.77	1.87	1.45	0.54	0.19
G-1*	175	2.0	90	25.4	19.5	1.57	1.63	2.31	3.70	0.95	0.12
"D"†		2.5	25	24	10	1.72	1.81	1.04	0.82	1.74	0.10
O-3	150	2.0	200	28.8	10	1.20	1.68	1.38	1.01	0.24	0.14
O-3	150	2.0	200	28.8	20	1.64	0.94	4.49	1.84	0.46	0.23
C-5	450	1.75	333	22.5	10	1.22	1.15	2.73	1.37	0.21	0.27
HR-4	81	6.75	27	24.5	10	2.04	0.82	0.37	0.13	0.25	0.037
M-1	70	2.0	100	19	10	1.75	1.06	0.65	0.30	0.16	0.065
U-1	60	2.0	8	25.8	15	11.9	0.42	0.43	0.08	0.53	0.029
U-1	60	20.3	81	25.3	15	1.83	2.32	2.24	2.27	1.44	0.149

*6 in. I.D. column. All other results, 4 in. column.
†Equal weight mixture of 41, 75, and 175 μ glass beads.

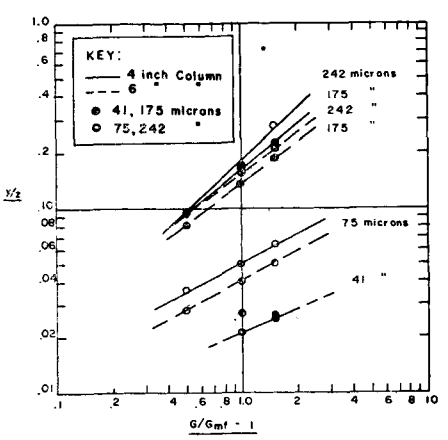

Fig. 5. Average y/z ratio for glass beads.

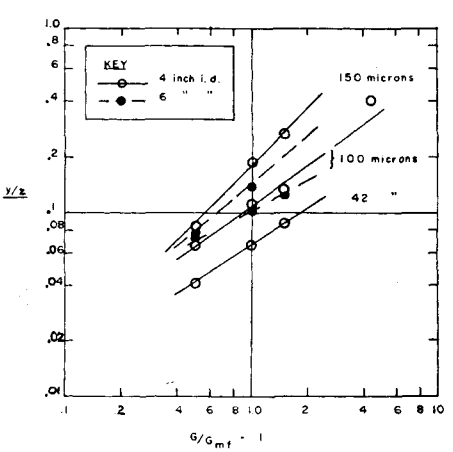

Fig. 6. Average y/z ratio for olivine.

Procedure

In all experiments solids were fluidized at room temperature and atmospheric pressure. The light probes were lowered into position when the bed was fluidized, and under steady state conditions oscillograms of the light signals from the probes were taken over ½- to 1-min. periods with the chart speed at 125 mm./sec. Speeds of 5 and 25 mm./sec. were also employed to check bubble frequency.

In most cases the air flow rates ranged from reduced mass velocities (defined as the ratio of mass velocity to minimum fluidization velocity) of 1.5 to 2.5, although a few higher air velocities were employed in the cases of olivine, hollow resin, UOP, and FCC catalysts. Bed heights measured at minimum fluidization ranged from 1 to 2.5 ft. The location of the probes varied from 5 to 25 in. above the bed support, depending upon the bed height. With one exception all runs were made with the probes at the axis of the column. The order of experimental treatments was randomized where practical to minimize statistical bias. Groups of runs for a given material were designed as factorial experiments.

The average characteristics of the air pockets or bubbles in the fluidized beds were calculated from measurements of the signal traces on the oscillograms. A particular tracing shown in Figure 2 will illustrate the method of calculation; channel 1 traces indicate light signals from the lower probe pair, and channel 2 traces the signals from the upper pair. The measured difference A-A', or t_1, represents the signal wave-front time lag, and the distance B-B', or t_2, corresponds to the wave-rear time lag. The time lag was obtained by averaging all the t_1's and t_2's for a given run; this represents the average time taken by the bubbles to rise the 1-in. distance from the lower to the upper probes. With the chart speed at 125 mm./sec. and the time lag in millimeters the average rise speed of the air bubbles was computed by the formula

$$v = \frac{1/12}{t/125} = 10.42/t \text{ ft./sec.} \quad (1)$$

The average thickness or vertical dimension of the bubbles was found from the average width

$$y = w/t \quad (2)$$

which gives y in inches for the distance between lower and upper probes of 1 in. and w and t in consistent units. For vertical probe separation differing from 1 in. these equations would be multiplied by the probe separation in inches. For air bubbles of a thickness less than about 2 in. significant corrections obtained from calibration data

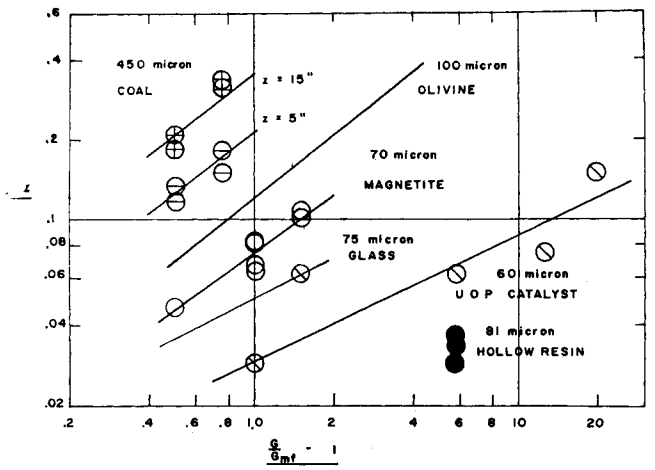

Fig. 7. Average y/z ratio for various materials in 4-in. column.

were employed. The average bubble frequency per second was determined by counting the number of signals and dividing by the elapsed time in seconds.

Since the average widths or horizontal dimensions of the air bubbles were not determined in these experiments, the present data do not afford a direct measurement of the volume or quantity of bubbles. Comparison with the work of Baumgarten and Pigford, however, suggests that vertical and horizontal bubble dimensions do not differ greatly.

An estimate can also be made on the basis of the data taken at the column axis. In this estimate of the volumetric flow rate of air bubbles, the bubbles were assumed to be uniformly distributed over the cross-sectional area of the column. If A_c is the column cross section in square feet and A_p is the horizontal projected area between the probe elements in square feet, then

$$Q_b = \frac{60nyA_pA_c}{12A_p}$$

$$= 5nyA_c \text{ cu. ft./min.} \qquad (3)$$

RESULTS

Figures 2 and 3 show two examples of the types of light-signal traces obtained at a chart speed of 125 mm./sec. for the 242- and the 75-μ glass beads, respectively. The irregular traces which have been obtained may indicate a rain of solid particles falling through the air pockets. Occasionally the oscillograms do not show a corresponding signal trace on the two channels, but this is not surprising in view of the dynamic system in which the air bubbles occur. Pulsations in the flow of air, particularly under slugging conditions, may give widely different time lags. The circulation pattern may cause bubbles to travel askew, or even downward. Many other considerations enter into the interpretation of the oscillograms.

Table 2 is an indication of the type of data obtained. Each line of bubble data represents the average results of measurements of a number of bubble traces. For example, the average number of bubble

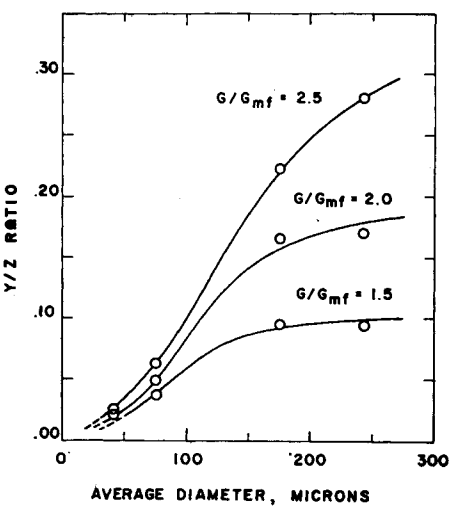

Fig. 8. Effect of particle diameter on bubble size ratio, glass beads in 4-in. column.

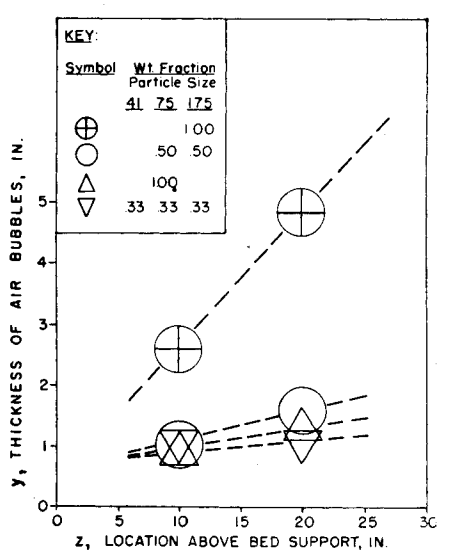

Fig. 9. Bubble thickness for mixed sizes of glass beads, $G/G_{mf} = 2.5$.

measurements for thickness is forty-six. Of a total of 375 such sets ten were based on fewer than ten bubbles, nineteen on fewer than twenty bubbles, and five on more than one hundred bubbles. Although this procedure decreased the standard deviation considerably, it is still fairly high when compared with physical measurements of typical nonstatistical nature. In the figures the large size of the symbols indicates the approximate standard deviation of the ordinate values. Complete composite data, of which Table 2 comprises less than 10%, are available as Tables 2 to 15 of reference *14*.* The system code number represents the type of solid material and the run series, with symbols defined in the notation. The first six columns represent operating conditions, the next three under *average bubble data* represent the primary result of this work, namely the gas-pocket rise speed, numerical frequency, and vertical pocket thickness. These will be analyzed separately. The last three columns of Table 2 are discussed later.

The factorial design approach used in the planning and execution of the experiments afforded a convenient means of estimating the level of significance of the effect of each controlled variable upon the measured results and the degree of interaction. Standard deviation estimates were based upon duplicate results and higher order interactions (*13*). By this means it was found that over-all bed height was not a significant variable; the type of bed support is discussed later. The column diameter and radial position of the probe were found to be significant factors, but investigation of these factors was of limited extent. The major variables influencing the characteristics of the rising gas pockets were type of particle (roughness, density, etc.), particle size, vertical position of the probes, and mass velocity of gas. It may be noted that bubble expansion owing to decrease in pressure as the bubble rises is negligible compared with the magnitude of the effect of probe height found in this work. Since air at 1 atm. is the only gas investigated thus far, no information on the influence of gas properties is available.

Average Bubble Thickness

Generally the average thickness of the air bubbles was found to increase with increases in air flow rate, position above the bed support, particle diameter, and particle density. As shown in Figure 4 for the 242-μ glass-beads system, y appeared to be a linear function of the height above the bed support. For clarity, points are omitted for G/Gmf = 2.0. Extrapolation of the curves to the point of origin indicated that y approached very small values. As an approximation in view of the large error variance straight lines were drawn from the origin of y vs. z graphs to follow the experimental points; the average y/z ratios were obtained from the slopes of these lines at various gas velocities. The effect of the bed height was not significant.

*Available as microfilm or photostats from University Microfilms, Ann Arbor, Michigan.

When these average y/z ratios were plotted against $G - G_{mf}$ or $(G - G_{mf})/G_{mf}$ on logarithmic coordinates, straight lines with different slopes and intercepts resulted for the various particle sizes investigated (Figures 5, 6, and 7). From the data for glass beads and olivine systems the following empirical equation was derived:

$$y/z = Bd^m(G/G_{mf} - 1)^{Ce^{0.002d}} \qquad (4)$$

Values for B, m, and C for glass beads are 0.00012, 1.4, and 0.35, respectively; for olivine the values are 0.003, 0.8, and 0.5; for the 6-in. column, B values are about 15% lower.

In Figure 8 the effect of particle diameter on the y/z ratio is shown more clearly to be rather complex. The apparent approach to asymptotic values indicated by Figure 8 for glass spheres was not brought out by the olivine data; however an extension of the data beyond the present scope may reveal a similar trend for such crushed material.

The lines for various materials in Figure 7 appear to be arranged mainly as a function of particle diameter. The low position of spherical hollow resin relative to spherical glass beads suggests y/z also increases with particle density. Comparison of the glass sphere, olivine rock, and magnetite data indicate the importance of other factors such as particle shape and size distribution; this study did not attempt to investigate such variables exhaustively. The following equation, of simpler form than Equation (4), incorporates the influence of particle density. It represents the data for all solids studied, although the coefficient of variation (percentage of standard deviation) is 56%.

$$\frac{y/z}{\rho d} = 1.6\left(\frac{G - G_{mf}}{G_{mf}}\right)^{0.63} \qquad (5)$$

Two size mixtures of glass beads were investigated to determine the effect of size distribution on air-bubble characteristics. Mix C consisted of an equal-weight mixture of 75- and 175-μ glass beads, mix D of an equal weight mixture of 41-, 75-, and 175-μ glass beads. The effects of these mixtures on the average bubble thickness may be seen in Figure 9, which shows that at $G/G_{mf} = 2.5$ the bubble size for the mixtures is less than that expected on the basis of average particle size alone. This particular effect is similar to that depicted in Figure 12 in the paper by Morse and Ballou (*2*).

RISE SPEED OF BUBBLES

For practically all the materials within the scope of the experiments the average rise speeds of air bubbles in the fluidized beds ranged between 1 and 2 ft./sec. The effects of many of the variables were minor, being masked by the relatively large error variance. For example the difference in rise speed between the approximately 40-μ-diameter glass beads and olivine illustrated in Figure 10 was

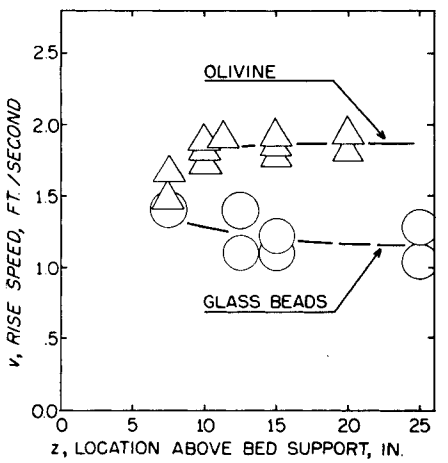

Fig. 10. Comparison of rise speed, 42-μ olivine and 41-μ glass beads in 4-in. column, G/G_{mf} of 2.0 and 2.5.

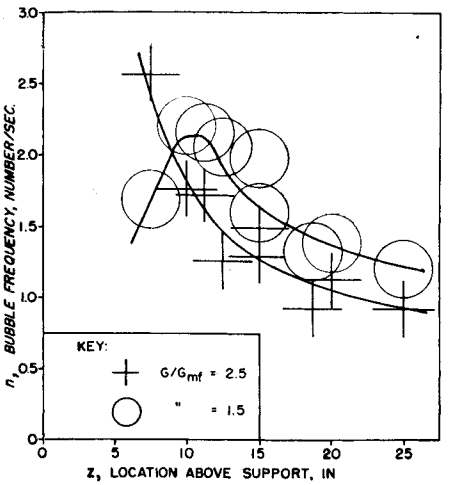

Fig. 11. Bubble frequency for 175-μ glass beads, 4-in. column, L_{mf} = 1.5 to 2.5 ft.

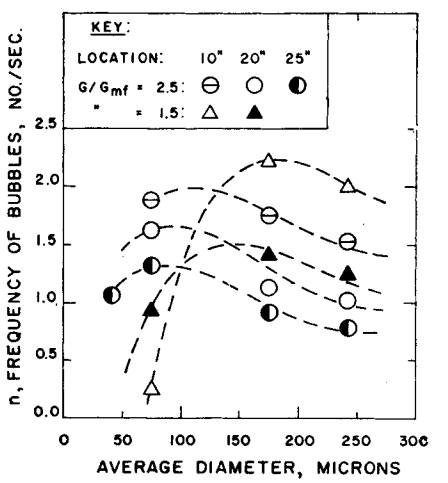

Fig. 12. Combined bubble-frequency data, glass beads in 4-in. column.

not noticeable for the larger sizes of the two materials. This graph of average bubble rise speed vs. location of the probes above the bed support indicates that the effect of the probe height is small except perhaps just above the bed support. Data for other systems show a slight increase of bubble velocity with position above the support in some cases and no change in others.

There was a small increase in the rise speed as the air velocity was increased for a given material. However the values of the rise speeds did not depend upon the absolute magnitude of the gas velocities. For the UOP catalyst system the rise speed of air bubbles was found to be greater than the average total gas velocity, which is defined as the superficial velocity divided by the void fraction. The coal-air system data yielded bubble velocities approximately equal to the average gas velocity.

On the basis of buoyancy the rise speed of bubbles would be expected to increase with increasing bed density, but such a trend was not clearly discernible. Other factors, such as bed viscosity and solids circulation, may affect the bubble velocity. The *wall effect* probably acts as a drag force to slow down large air bubbles, for the solids are pushed out of the way and flow down countercurrent to the rising mass of air when the bubble is large with respect to the column diameter. The relatively constant bubble velocity found for the fluidized beds is similar to the behavior of gas bubbles in a given liquid in which the drag coefficients and wall effects are such as to give only a small increase in bubble velocity with increase in bubble size, within the ordinary range of bubble diameters. In gas-liquid systems however liquid density and viscosity have a pronounced effect on the rate of rise of bubbles.

In view of the large range of particle density, particle size, and air velocity used in this work these considerations can be only a partial explanation of the limited range of rise speed. The data strongly suggest that the major factor influencing the rate of rise is the rate of fall of the particles through and around the low density region. The irregularities of oscillograph traces show that considerable quantities of *solids may rain* down through the void regions. Since gas velocity in most fluidized beds is a small fraction of the free fall velocity of the particles, those particles no longer supported from below by the dense phase could accelerate downward at a rate dependent mainly upon the earth's gravitation. If it is assumed that particles are essentially at rest at the roof of the void and fall freely through the ¾ to 4 in. of bubble height, the average velocity of bubble rise (or particle fall) would range from 1.0 to 2.3 ft./sec., which is the same magnitude as the velocity observed. If this is the mechanism of bubble rise, it would suggest there is much less by-passing of the solid by the gas than the actual volumes of the bubbles.

TABLE 3. EFFECT OF BED SUPPORT ON BUBBLE CHARACTERISTICS

Run 4-GAS-1 — 175 μ glass beads; Column diameter = 4 in.; L_{mf} = 2 ft.; Probe spacing, s = ¼ in.; G_0: G/G_{mf} = 1.5; G_1: G/G_{mf} = 2.5; z_0 = 10 in.; z_1 = 20 in.

Code	Porosity μ	Thickness in.	Material	G_0 Z_0	G_0 Z_1	G_1 Z_0	G_1 Z_1
	Type of bed support			Average characteristics			
				Rise speed, ft./sec.			
A	20	⅛	Porous stainless steel	1.19	1.50	1.21	1.69
B	55	1½	Porous ceramic	1.38	1.55	1.25	1.77
C	55	½	Porous ceramic	1.25	1.42	1.33	2.11
D	110	1½	Porous ceramic	1.42	1.45	1.30	1.94
E	110	½	Porous ceramic	1.27	1.44	1.33	1.90
F	74	.002	Screen, stainless steel	1.16	1.57	1.18	1.74
			(Average)	1.28	1.49	1.27	1.86
				Thickness, in.			
A	20	⅛	Porous stainless steel	1.09	2.45	3.18	4.90
B	55	1½	Porous ceramic	1.04	2.31	2.31	4.52
C	55	½	Porous ceramic	0.96	2.07	2.94	5.71
D	110	1½	Porous ceramic	1.11	2.09	3.20	5.13
E	110	½	Porous ceramic	1.21	2.33	2.50	5.37
F	74	.002	Screen, stainless steel	1.31	2.89	2.88	4.77
			(Average)	1.12	2.36	2.84	5.07
				Frequency, No./sec.			
A	20	⅛	Porous stainless steel	1.94	1.35	1.36	1.13
B	55	1½	Porous ceramic	2.44	1.40	1.98	1.21
C	55	½	Porous ceramic	2.27	1.41	1.74	1.12
D	110	1½	Porous ceramic	2.00	1.38	1.59	1.10
E	110	½	Porous ceramic	2.16	1.32	1.88	1.04
F	74	.002	Screen, stainless steel	1.54	1.15	1.63	1.25
			(Average)	2.06	1.34	1.70	1.14

TABLE 4. BUBBLE-SIZE DISTRIBUTION-RUN 4-GA-6

Trace width or trace height, mm.	Number of observations of trace width at G/G_{mf} equals 1.25	1.5	1.75	2.0	of trace height at G/G_{mf} equals 1.25	1.5	1.75	2.0
0–5	30	7	7	0	72	30	23	5
5–10	96	44	17	6	38	33	21	12
10–15	13	71	30	10	16	36	21	21
15–20	0	38	47	22	11	20	19	31
20–25	0	3	32	31	6	26	28	16
25–30	0	1	2	21	3	13	21	11
30–35	0	0	0	11	3	6	2	5
Total No.	139	164	135	101	139	164	135	101

Data from Run 4-GA-6, 242 μ glass beads in 4 in. column, probes at 20 in.

TABLE 5. EFFECT OF HORIZONTAL PROBE SPACING ON MEASUREMENT OF AVERAGE BUBBLE CHARACTERISTICS

	Average bubble characteristics: Rise speed, ft./sec.				Thickness, y, in.				Frequency, No./sec.			
G/G_{mf}	1.5		2.5		1.5		2.5		1.5		2.5	
Z, in.	10	20	10	20	10	20	10	20	10	20	10	20
Probe spacing, in.												
¼	1.23	1.31	1.07	1.59	0.81	2.04	2.58	5.52	2.08	1.30	1.64	1.06
⅝	1.63	1.34	1.06	1.49	0.85	1.61	1.67	4.46	1.34	1.19	1.94	1.04
1	1.98	1.31	0.98	1.62	0.81	1.22	1.34	4.06	0.66	0.91	1.37	1.09

Data from Run 4-GA-7, 242-μ glass beads in 4-in. column.

Bubble Frequency

The observed air-bubble frequencies in the present experiments ranged from 0 to almost 3 bubbles/sec. Detection of air bubbles by the probes depends to some extent on the spacing between the lamp and the reflecting prism, upon the location of the probes with respect to the bulk of the bubbles in the bed, and upon the size of the bubbles. Probe spacing between the lamp and reflecting prism was ¼ in. except for a special investigation of this variable discussed later. It was found that bubbles smaller than about ½ in. could not be detected easily, and consequently bubble-frequency data are low and probably not reliable for bubble thicknesses of less than ½ in. Quite apart from the difficulty of detecting very small bubbles the data indicated a decrease in the number of bubbles as their dimensions increased, suggesting that bubbles grew in size by coalescing. Analysis of variance indicated much interaction of the effects of operating variables upon frequency. A correlation of factors contributing to detected frequency was not found. For the glass beads the type of curves shown in Figure 11 appear to relate bubble frequency with the location of the probes above the bed support. The 175 μ glass beads system shows for G/G_{mf} = 1.5 a typical increase in frequency starting from a low bed height (small bubble size) and then after a maximum value decreasing in an exponential manner. The zone of decreasing frequency is attributed to the rate of bubble coalescence. At the higher ratio of G/G_{mf} the bubbles were already large and therefore readily detectable in the range shown, so that the zone of increasing frequency is not present; this is born out by the data for other sizes of glass beads.

Figure 12, showing the average bubble frequency as a function of average particle diameter for glass beads in the 4-in. column, illustrates the complex relationship existing. The shapes of these curves are explained by previous considerations and by recalling that bubble size increased with particle size, location above the bed support, and increasing gas velocity.

If consideration is restricted to conditions giving bubble thicknesses of 1 in. and greater, gas velocity does not appear to greatly affect the average bubble frequency. More detailed results may be found in reference (*14*).

Other Considerations

Separate investigations show the influence of bed support on gas pocket characteristics, the effect of horizontal light source-to-prism spacing of the probes, and the effect of radial position of the probes. The trace width and trace height distribution (which correspond to gas pocket height and diameter, respectively) were also investigated for 242-μ glass beads.

Table 3 compares five porous plate bed supports of varying thickness and pore diameter and one 200-mesh screen for their influence on average bubble rise speed, thickness, and frequency. The differences between the types of support are statistically significant for this and similar data at other conditions only for the effect of the screen upon bubble frequency. Since drilled plate supports were not investigated, comparison with the porous plates and screen used in this

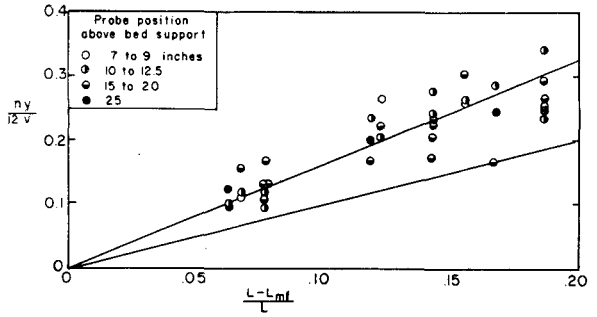

Fig. 13. Comparison of fractional voids within bed as entrained bubbles vs. bed expansion, 242-μ glass beads.

work is not possible. The larger hole size and spacing of most drilled plates or grids would probably influence not only bubble frequency but bubble size as well. Others have observed differences in fluidization uniformity between grids and porous plates, at least near the bed support. The major purpose of the bed support investigation in this work was to insure that unknown variations in bed support would not influence the results. Ceramic disk supports 1½ in. thick with 55-μ mean pore diameter were used for the major experimental work. For the conditions of Table 3 pressure drop through this plate (B) ranged from 50 to 100% of the pressure drop through the bed proper. For porous plates A, C, and D comparable values ranged from 4 to 20%, while for plate E and screen F values were approximately 1%.

Table 4 summarizes measurements of the statistical variation of gas pocket size. Counts were made of trace size in 5-mm. increments. Trace width corresponds to the time a gas pocket is between the lower probe pair or its vertical thickness. Trace height is a measure of the light transmitted at the peak of the trace. A high trace indicates a pocket at least as large in diameter as the distance between probes (⅝ in.); a smaller trace indicates a pocket of smaller diameter or one containing solid particles. The edge of a large bubble would result in smaller trace length and width. The results therefore are only an approximate indication of pocket size. Replicate runs served to show the existence of a common variance for the various data by Bartlett's test (*17*). Table 4 indicates the range of data which were averaged to obtain results such as found in Table 2.

A related investigation was that for the effect of probe spacing from light to prism upon measurements of bubble characteristics. The data and analysis of variance indicate an effect of probe spacing on bubble frequency and thickness strongly dependent on the level of the factors z and G. Table 5 indicates some of the results. The influence of probe spacing upon bubble frequency is significant at low mass velocity and low probe height. Under these conditions gas pockets are small, and the larger probes do not detect the smaller pockets. For this reason ¼-in. probe spacing was used in the major experimental work; even this probe spacing may fail to detect the smallest bubbles present at low probe height and low mass velocity. This is also a limitation of other detecting devices which have been reported such as electrical capacitance probes and X-ray technique. With the latter technique there is a possibility of classifying a number of such small bubbles in the ray path as a single larger bubble. Fortunately such small bubbles would be of secondary importance in by-passing or bed uniformity. The decrease in observed bubble thickness for wide probe spacing may reflect the short time that a bubble completely fills the zone between widely spaced probes. Again the use of small probe spacing should minimize this difficulty.

Discussion

A speculative description of the nature of flow in a gas-fluidized bed can be based upon the results obtained. Almost immediately upon increasing gas flow beyond minimum fluidization velocity, regions of low solid density begin to form. These regions are small near the bed support, and their diameter increases as they rise by coalescence of smaller bubbles. The diameter of such regions is increased by increasing particle size, particle density, and gas flow rate and by decreasing particle-size range. With the column sizes used in this work total bed height was not a significant variable. The bubbles are extremely irregular in outline and relatively nonuniform in size.

For bubbles larger than about ¾ in. detected frequency decreases with increasing probe height, thus suggesting growth by coalescence. For materials such as cracking catalyst and hollow resin, which are characterized by *smooth* fluidization, bubble frequency increased with increasing air velocity. For larger, heavier particles frequency is relatively unaffected by increasing air flow rate. Bubbles in such media tend to coalesce easily and grow large.

The rate of rise of bubbles is only moderately affected by operating conditions. For laboratory scale systems such as those studied in this work this may be in part the result of wall effect and solids circulation patterns. The major explanation proposed is that voids are moved upward mainly by collapse of the solids through and around the voids. At ordinary fluidization velocities the rate of collapse approaches that resulting from gravitational attraction of the solid.

The product of bubble frequency and size should be a measure of the volume of gas passing through the bed in the form of bubbles. This product divided by the average bubble velocity and by the column cross-sectional area should represent the volume fraction of gas as bubbles retained within the fluidized bed at any time. The latter is plotted vs. the fractional bed expansion $(L\text{-}Lmf)/L$ in Figure 13 for 242-μ glass beads. If the bed expansion is due entirely to the presence of bubbles in the bed, the ordinate and abscissa values should agree; if the dense phase of the bed is expanded, the abscissa should exceed the ordinate value. It is apparent that the volume of bubbles retained within the bed, as calculated from the data, correlates with the fractional bed expansion but equals or exceeds this value in every case. On the basis of Figure 13 it may therefore be concluded conservatively that the dense-phase portion of the bed remains at essentially the density found at minimum fluidization velocity. The figure indicates that the group $ny/12v$ may be too large, since it is difficult to visualize the dense phase being fluidized with less air than required at minimum fluidization velocity. The most probable reason for large values of this group is that gas bubbles preferentially seek the center of the bed, and the center-line probe therefore yields size data greater than the average value over the cross-sectional area. The points plotted show no consistent trend with the height of the probe above the bed support, a further indication that the volume of gas as bubbles remains constant vs. bed height, bubbles being more frequent at low levels but larger at high levels.

The ratio of gas flowing as bubbles to that required to fluidize is plotted vs. $(G\text{-}Gmf)/Gmf$ in Figure 14 for the same solid used in Figure 13. The abscissa represents gas flow in excess of

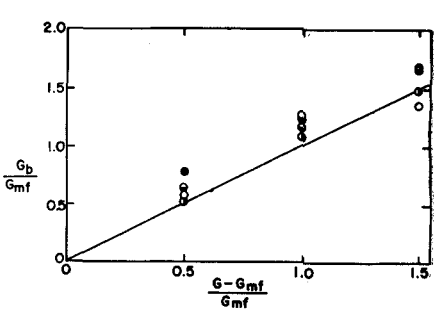

Fig. 14. Comparison of bubble flow rate vs. excess fluidizing gas, 242-μ glass beads.

minimum fluidization. If the two-phase theory of fluidization (*18*) were followed in its strictest sense, this quantity should be equal to the ordinate value. Since Figure 13 indicated that measured bubble volumes were probably higher than average values for the entire bed, the ordinate values shown in Figure 14 are also probably somewhat high. It is evident from these results that the measured bubble volume is about that expected, if all gas in excess of minimum fluidization velocity were in the form of bubbles. *Data of* Figure 14 for 242-μ glass beads correlated better than most data plotted similarly, but the same qualitative results were evident for most of the systems studied. Typical values of G_b/G are shown in Table 2.

The recent work of Baumgarten and Pigford (*5*) closely parallels the present work; these authors measured the instantaneous bed density in a rectangular column by the extent of gamma-ray absorption, with a technique similar to that of Grohse (*6*). Baumgarten and Pigford were able to deduce values representing bubble diameter (horizontal width), bubble frequency, and bubble rate of rise. The rise rate was obtained indirectly, from a knowledge of bubble frequency; bubble width was obtained from the instantaneous density at a trace peak and time average bed density. Solids used were glass beads of about the same size ranges as used in this work and a fluid cracking catalyst.

In agreement with this work they found bubble-size increases with gas velocity, height above bed support, and particle size. Although results were not conclusive, bubble frequency appeared to decrease somewhat with probe height in agreement with this work. They observed a marked, though somewhat erratic, influence of distance from the wall upon bed density and bubble frequency. This variable was not explored appreciably in the present work.

They conclude from their work that the rate of rise of bubbles increases rather markedly with increasing probe height. This conclusion nesessitates postulating a transfer of gas from the dense phase to bubble phase as the gas rises through the bed, since bubble size and frequency do not decrease correspondingly. The present work is not in agreement with this conclusion; rather it postulates a minor change in rise speed with probe height and relatively constant total gas volume vs. probe height. Additional work may clarify this point. Although both investigations indicate increase in bubble size with height above support, Figure 7 of the work of Baumgarten and Pigford does not readily extrapolate to zero at the bed support as does the present work.

Ohmae and Furukawa (*12*) photographed bubbles in a rectangular column. The technique suffers somewhat in restricting observation to bubbles adjacent to the wall. These authors found the volume of gas as bubbles increased, though not linearly, with total gas flow. They also found bubbles to grow sufficiently to cause slugging at a lower total bed height for increasing gas velocity. This is consistent with bubble size increasing with both gas velocity and height above bed support. Zenz (*19*) has interpreted slugging to represent growth of bubbles to column diameter size. Bubble diameters determined in this manner from the work of several authors increase with bed height and particle diameter in agreement with work previously discussed. Quantitative comparison of bubble sizes is uncertain because results in general do not specify the gas velocity as well as the bed height for slugging conditions.

In conclusion, data on gas-bubble characteristics for a variety of materials are presented. In agreement with the limited available results of other authors, these data show gas bubbles to increase in size with particle size, probe height, and gas velocity and to decrease in frequency with probe height. It is postulated without verification by other work that though bubble size increases with probe height by coalescence, the quantity of gas as bubbles remains substantially constant. The rise velocity was also found to remain relatively constant with probe height in disagreement with the conclusions of Baumgarten and Pigford.

ACKNOWLEDGMENT

The authors are indebted to The Texas Company, represented by Roland Beck, for financial support of this work.

NOTATION

A_c = cross sectional area of column, sq. ft.
A_p = horizontal, projected area covered by probe elements, sq. ft.
B = constant in Equation (4)
C = constant in Equation (4)
D_c = diameter of column, in.
d = average diameter of particle based on surface, μ [ft. in Equation (5)]
e = base of natural logarithm
G = mass velocity of air, lb./(hr.)(sq. ft.)
G_{mf} = minimum fluidization velocity, lb./(hr.)(sq. ft.)
G_0, G_1 = levels of air velocity
G_b = mass velocity of air bubbles, lb./(hr.)(sq. ft.)
L = bed height above support, in. or ft.
L_{mf} = bed height at minimum fluidization, in. or ft.
n = average frequency of air bubbles, No./sec.
m = constant in Equation (4)
Q_b = volumetric flow rate of air bubbles, cu. ft./min.
t = average time lag of channel 1 and 2 traces, mm.
v = average rise velocity of air bubbles, ft./sec.
w = width of oscillogram trace, mm.
y = average thickness, or linear dimension measured vertically, of the air bubbles, in.
z = height of probes above bed support, in.
ρ = particle density, lb./cu. ft.

Run Code Letters

A = air
C = coal
D = mixture
G = glass beads
MR = hollow resin
M = magnitite
O = olivine
S = support variation run
U = UOP catalyst

LITERATURE CITED

1. Morris, J. B., J. B. Nicholls, and F. W. Fenning, *Trans. Inst. Chem. Engrs. (London)*, **34**, 168 (1956).
2. Morse, R. D., and C. O. Ballou, *Chem. Eng. Progr.*, **47**, 199 (1951).
3. Dotson, J. M., Paper presented at the Chicago AIChE Meeting, December, 1957.
4. Schuster, W. W., and Peter Kisliak, *Chem. Eng. Progr.* **48**, 455 (1952).
5. Baumgarten, P. K. and R. L. Pigford, Paper submitted to the *A.I.Ch.E. Journal*, 1957.
6. Grohse, E. W., *A.I.Ch.E. Journal* **1**, 358 (1955).
7. Dickman, Robert, and W. L. Forsythe, *Ind. Eng. Chem.*, **45**, 1174 (1953).
8. Furukawa, Junji, and Tsutomu Ohmae, *J. Chem. Soc. Japan, Ind. Chem. Sect.*, **54**, 798 (1951).
9. Matheson, G. L., W. A. Herbst, and P. H. Holt, *Ind. Eng. Chem.* **41**, 1099 (1949).
10. Fritz, J. C., Jr., Ph.D. thesis, Univ. Wisconsin, Madison (1955).
11. Mathis, J. F. and C. C. Watson, *A.I.Ch.E. Journal*, **2**, 578 (1956).
12. Ohmae, Tsutomu, and Junji Furukawa, *J. Chem. Soc. Japan, Ind. Chem. Sect.* **56**, 909 (1953).
13. Davies, Owen L., ed., "The Design and Analysis of Experiments," Hafner Pub. Co., New York (1956).
14. Yasui, George, Ph.D. thesis, Univ. Washington, Seattle (1956).
15. Ergun, Sabri, *Chem. Eng. Progr.* **48**, 89 (1952).
16. Heywood, Harold, *Symp. on Particle Size Analysis, Trans. Inst. Chem. Engrs. (London)*, 25, **14** (1947).
17. Ostle, Bernard, "Statistics in Research," The Iowa State College Press, Ames (1954).
18. Toomey, R. D., and H. F. Johnstone, *Chem. Eng. Progr.* **48**, 220 (1952).
19. Zenz, F. A., *Petroleum Refiner*, **36**, No. 4, 173 (1957).

Manuscript received December 18, 1957; revision received May 13, 1958; paper accepted May 13, 1958.